Simultaneous formation of CH3NH3PbI3 and electron transport layers using antisolvent method for efficient perovskite solar cells

Chunfeng Lan, Huabin Lan, Guangxing Liang, Jun Zhao, Huanxin Peng, Bo Fan, Zhuanghao Zheng, Huibin Sun, Jingting Luo, Ping Fan, Yong Qing Fu

PII: S0040-6090(18)30386-9
DOI: doi:10.1016/j.tsf.2018.05.052
Reference: TSF 36695

To appear in: *Thin Solid Films*

Received date: 15 February 2018
Revised date: 15 May 2018
Accepted date: 30 May 2018

Please cite this article as: Chunfeng Lan, Huabin Lan, Guangxing Liang, Jun Zhao, Huanxin Peng, Bo Fan, Zhuanghao Zheng, Huibin Sun, Jingting Luo, Ping Fan, Yong Qing Fu , Simultaneous formation of CH3NH3PbI3 and electron transport layers using antisolvent method for efficient perovskite solar cells. Tsf (2017), doi:10.1016/j.tsf.2018.05.052

Simultaneous Formation of $CH_3NH_3PbI_3$ and Electron Transport Layers Using Antisolvent Method for Efficient Perovskite Solar Cells

Chunfeng Lan[a,b,c], Huabin Lan[a,c], Guangxing Liang[a,c], Jun Zhao[a,c], Huanxin Peng[a,c], Bo Fan[a,c], Zhuanghao Zheng[a,c], Huibin Sun[a,b,c], Jingting Luo[a,c*] and Ping Fan[a,c*], Yong Qing Fu[d]

[a.] Shenzhen Key Laboratory of Advanced Thin Films and Applications, College of Physics and Energy, Shenzhen University, 518060 Shenzhen, China

[b.] Key Laboratory of Optoelectronic Devices and Systems of Ministry of Education and Guangdong Province, College of Optoelectronic Engineering, Shenzhen University, Shenzhen 518060, China

[c.] Institute of Thin Film Physics and Applications, College of Physics and Energy, Shenzhen University, Shenzhen518060, China

[d] Faculty of Engineering and Environment, Northumbria University, Newcastle upon Tyne, NE1 8ST, UK

* Correspongding author: E-mail:luojt@szu.edu.cn(Prof. Luo), fanping308@126.com (Prof. Fan)

Abstract: A new antisolvent method was developed to prepare $CH_3NH_3PbI_3$ and electron transport layers for making efficient hybrid perovskite solar cells. By directly using [6,6]-phenyl-C61-butyric acid methyl ester in chlorobenzene solution as antisolvent, $CH_3NH_3PbI_3$ and electron transport layers were simultaneously formed in the films. This method not only simplifies the fabrication process of devices, but also produces uniform perovskite films and improves the interfacial structures between $CH_3NH_3PbI_3$ and electron transport layers. Large perovskite grains were observed in these films, with the average grain size of more than 1 μm. The so-formed $CH_3NH_3PbI_3$/electron transport layers demonstrated good optical and charge transport properties. And perovskite solar cells fabricated using these simultaneously-formed layers achieved a higher power conversion efficiency of 16.58% compared to

conventional antisolvent method (14.92%). This method reduces nearly 80% usage of chlorobenzene during the fabrication, offering a more facile and environment-friendly approach to fabricate efficient perovskite solar cells than the conventional antisolvent method.

Keywords: Antisolvent method; Simultaneous formation; Perovskite solar cells; Crystallization; Photovoltaic performance.

Introduction

Halide hybrid perovskite solar cells have attracted considerable attention in the field of thin-film photovoltaics due to their low-cost process and high power conversion efficiency (PCE) [1-4]. Their certified PCE has now rapidly reached up to 22.1% in the past seven years [5]. During the development of perovskite solar cells, the film quality of perovskite and their associated functional layers, including electron and hole transport layers, have been proven as the key issues in achieving high-performance devices [1,6-8]. Many methods, such as two-step chemical solution method, one-step chemical solution method and vacuum-based physical vapor deposition methods, have been introduced to prepare the perovskite layers [9-11]. In the past two years, the antisolvent method which uses chlorobenzene (abbreviated as CB), toluene, ether or dichlorobenzene as the antisolvent to quickly crystallize the perovskite films, has been verified as a facile and effective method for preparing high-quality perovskite films [12]. The devices fabricated using this method have achieved a PCE of over 20% [12]. Meanwhile, [6,6]-phenyl-C61-butyric acid methyl ester (PCBM) has been identified as an effective electron transport layer for efficient inverted perovskite solar cells, and its high charge mobility helps to minimize the hysteresis of the perovskite devices [13,14]. Even though perovkskite solar cells with inverted device structure exhibited a good photovoltaic performance, they still have some critical problems to be solved, for example, their fabrication process consumes numerous environmentally-toxic solvents, such as CB and N,N-dimethyl formamide (DMF). Therefore, it is critical to develop a relatively environment-friendly method to fabricate perovskite solar cells.

The conventional antisolvent method for preparing perovskite films is spin-coating mixtures of PbI_2, CH_3NH_3I, $HC(NH_2)_2I$ and CH_3NH_3Br [12]. And during the spin-coating process, antisolvents, typically CB, ether or toluene, are quickly dropped on the precursors, and then the as-prepared films are annealed to form absorbing layers. Afterwards, the PCBM pre-dissolved in the CB solution is spin-coated onto the perovskite film to form electron transport layer for inverted-structure perovskite solar cells [10,12-14]. These two steps consume the toxic solvent CB which is difficult to be decomposed in the environment and can cause cancer in human being [13]. Clearly it is necessary to reduce the usages of these toxic solvents and simplify the fabrication processes of perovskite solar cells.

In this work, by using the PCBM in CB solution (PCBM-CB solution) as antisolvent, we develop a simultaneous formation method for $CH_3NH_3PbI_3$ perovskite ($MAPbI_3$) and PCBM layers. This method dramatically simplifies the process and reduces the usages of chlorobenzene during the fabrication. The perovskite/PCBM layers prepared by this method exhibit high quality crystallization of perovskite films and good interfacial structures. The simultaneously-formed $MAPbI_3$ perovskite solar cells can achieve a high photovoltaic performance, with a PCE of 16.58%.

Experimental details

Materials: The following materials have been used: CH_3NH_3I (99%, MaterWin, China), PbI_2 (99%, Xi'an Polymer Light Technology, China), DMF (99.0%, MaterWin, China), Dimethyl sulfoxide (DMSO) (≥99.0%, MaterWin, China), CB (99.8%, Sigma-Aldrich, China), poly(3,4-ethylenedioxythiophene) polystyrene sulfonate (PEDOT:PSS) (Clevios, PVP AI4083, Germany), PCBM (99%, aladdin, China), Indium Tin Oxide glass (ITO) (Square resistance < 15 Ω, South China Xiangcheng Tech., China).

Preparation Method: Perovskite precursor (45 wt%) was prepared by adding a mixture of stoichiometric CH_3NH_3I and PbI_2 into a mixed solvent of DMF and DMSO(with a volume ratio DMF:DMSO of 4:1), and filtered for further usage. PCBM of 20 mg weight was diluted in the CB solution of 1 ml. As shown in Figure

1(a), the perovskite precursor with a volume of 60 µl was dropped onto a PEDOT:PSS layer and spin coated at 4000 rpm for 30 s, at 4 s during spinning 60 µl of the PCBM-CB solution was dropped onto the surface. Subsequently, the films were annealed at 120 ^{o}C for 20 min to form perovskite and PCBM layers (PCBM-perovskite). Meanwhile, as shown in Figure 1(b), perovskite films (CB-perovskite) were prepared using a conventional antisolvent method, in which they were processed with the pure CB solvents with volumes of 60 µl and 250 µl, respectively. For further comparisons, the CB-perovskite films were sequentially coated with the PCBM solution, and labeled as perovskite + PCBM.

Device fabrication: The PEDOT:PSS aqueous solution was spin-coated onto an ITO/glass substrate at a rotation speed of 3000 rpm for 30 s, and the resulting PEDOT:PSS film was annealed at 140 ^{o}C for 30 min. The perovskite and PCBM layers were prepared on the dried PEDOT:PSS layers using the method described above. For the conventional method to prepare perovskite and PCBM layers, 50µl of PCBM solution (with a concentration of 20 mg/ml) was spin-coated onto the perovskite layer at a rotation speed of 4000 rpm for 30 s. Finally, device fabrication was completed by thermal evaporation of a 100 nm thick Ag layer as the cathode.

Characterization of Films and Devices: X-ray diffraction (XRD,Ultima IV) was carried out to determine crystalline structures of the films with CuKα radiation(λ = 0.15406 nm) operated at 40 kV and 40 mA. Surface and cross-section morphologiesof the prepared films and devices were analyzed using a field-emission scanning electronmicroscope (FE-SEM, Zeiss, SUPRA 55). UV-visible spectrum transmittance and reflectance were measured using a spectrophotometer (UV-3600Plus, Shimadzu). Photoluminescence measurement was carried out using a time-resolved and steady-state spectroscope (FluoTime 300, PicoQuant GmbH) with a peak wavelength of 770 nm. Current density-voltage (*J-V*) characteristics of the perovskite solar cells were tested under a standard simulated light source AM 1.5G conditions (100 mW/cm^2) with a Keithley 2400 sourcemeter in ambient conditions. The voltage was forwardly and reversely scanned between 0 and 1.1 V with a scan rate of 0.1 V/s. The devices area illuminated was precisely set as 0.12 cm^2.

Results and Discussion

Figure 2 illustrates XRD patterns of the perovskite films prepared using different methods. Generally, all the samples reveal the key characteristic diffraction peaks of (110), (220), and (330) planes of $MAPbI_3$, which can be assigned to its tetragonal crystal structure [15]. Few peaks were found at 12.67° (i.e., the (001) diffraction peak of PbI_2) and 25.92° (i.e., the (101) diffraction peak of PbI_2), thereby indicating the complete formation of the preferred phases. Table 1 summarizes the XRD results of the films prepared through the newly proposed simultaneous formation method, and it shows the strongest intensity at the (110) peak, which is the preferred orientation of the perovskite. It is also noted that the Scherrer equation is only accurate for crystals smaller than 100 nm [16], in this case full-width at half-maximum (FWHM) and diffraction intensity were used to make a rough comparison on crystallization(the latter discussion shows large grain more than 100 nm). The FWHM of (110) reflection of PCBM-perovskite and CB-perovskite are 0.346 and 0.371 deg., respectively. Correspondingly, the (100) diffraction intensity of PCBM-perovskite is higher than that of CB-perovskite, indicating the better crystallization of PCBM-perovskite than CB-perovskite. The (004) peak of tetragonal $MAPbI_3$ crystal at 27.22 ° is found at PCBM-perovskite film, inferring its preferred C-axis orientation.

Figures 3(a,b) show the top-view FE-SEM images of the perovskite films prepared through conventional antisolvent method with different volumes of CB (250 ul and 60 ul). For the perovskite+PCBM film, it only shows the morphology of PCBM, without the detection of perovskite. The grain size statistics of perovskite films are shown in Figure 3(d) (calculated by Nano Measurement software) [17], and it is found that the grain sizes of CB-perovskite film are ranged between 100 nm and 700 nm (mean size of about 300 nm), with numerous grain boundaries. The surface of PCBM-perovskite shown in Figure 4(a) is similar to that of perovskite-PCBM. In order to make a comparison with CB-perovskite and understand the PCBM effect on $MAPbI_3$ formation, the PCBM-perovskite and perovskite+PCBM films were rinsed using CB to remove the PCBM layer, and then dried for FE-SEM detection.

Remarkably, Figure 4(b) clearly shows the PCBM-perovskite film have larger grains than CB-perovskite, and grain size statistic for PCBM-perovskite in Figure 4(d) indicates the mean size is over 1 μm. For the evaluation of the CB-rinsing effect on the morphology of perovskite films, the CB-rinsed perovksite+PCBM film in Figure 4(c) only shows a similar morphology as that of the CB-perovskite film, implying that the microstructure difference of the perovskite films might come from the antisolvent treatment process.

During the conventional antisolvent method, the DMF and DMSO solvent were extracted by the antisolvent; and the perovskites were quickly nucleated and developed on the surface [10,12]. During the perovskite formation, the hydrophobicity ability of PCBM could effectively reduce the interaction between polar solvent vapors and the perovskite nuclei [18]. Consequently, PCBM can suppress the nucleation of the perovskite due to the increase of the surface free energy [18-23]. Thereby, the PCBM-CB solution would passivate the formation of nano-grains during the simultaneous formation process. This helps to reduce the number of nucleate sites and then promote the growth of large perovskite grains [19]. Accordingly, in the XRD analysis the simultaneously-formed PCBM-perovskite film exhibited a relatively high intensity, indicating its good crystallinity. Figure 5 further shows the cross-sectional FE-SEM image of the simultaneously-formed layers, revealing that the perovskite and PCBM layers are perfectly bonded together through this newly developed method, in which the thicknesses of the PCBM and the perovskite layers are~60 and ~300 nm, respectively.

The microstructures of perovskite films can strongly affect their optical properties [24,25]. Figure 6 displays the UV-visible spectra of the perovskite films with and without using the PCBM in the process. The reflectance intensity of the CB-perovskite film in Figure 6(a) is slightly stronger than those of the simultaneously-formed PCBM-perovskite and perovskite+PCBM films. The high reflectance could be attributed to the minor effect of the conventional CB-perovskite films. Figure 6(b) illustrates that the transmittance spectrum of the simultaneously-formed PCBM-perovskite film is lower than that of the other films in

the long-wavelength region. This result is mainly due to the existence of few grain boundaries in the PCBM-perovskite film, which can reduce the light-scattering. Accordingly, the absorption spectra calculated from the reflectance and transmittance is shown in Figure 6c, indicate that the PCBM-perovskite and perovskite+PCBM films have a good absorption, and also the majority of absorption peaks starts at a wavelength of ~ 780 nm.

Besides the optical properties, the time-resolved photoluminescence (TRPL) analysis was also performed for these films. TRPL was reported as an effective method to evaluate the carrier lifetime of absorber and charge transport between absorbing and functional layers [25,26]. For PCBM-perovskite, CB-perovskite, and perovskite+PCBM on glass, the TRPL lifetimes were determined by measuring the PL decay of the emission peak wavelength at 770 nm, with an excitation wavelength of 532 nm (Figure 7). From these results, the charge lifetime and the charge-transport processes were investigated. The PL decay time ($\tau 1$) of glass/CB-perovskite was calculated to be 61 ns based on the decay values obtained using a bi-exponential method. The lifetimes for the glass/PCBM-perovskite and glass/perovskite+PCBM are much lower than that of the CB-perovskite film. These results clearly revealed the effective charge extraction from perovskite to PCBM layers in the perovskite/PCBM films. However, the PCBM-perovskite film shows a longer lifetime than the perovskite+PCBM films. Usually, there are two reasons to explain this phenomenon, one is the improved lifetime of absorbing layer itself, another is reduced charge extraction [27]. According to the XRD and SEM results discussed above, this can be attributed to the former one which is associated with improved film quality of perovskite. Compared to the CB-perovskite with numerous nano-grains, the simultaneously-formed PCBM-perovskite films has much fewer grain boundaries, which significantly reduces the non-radioactive recombination of the photo-excited electron-hole pairs and benefits a long lifetime in the absorbing layer [28].

Using the simultaneously-formed PCBM-perovskite and the conventionally processed perovskite+PCBM layers, perovskite solar cells were fabricated based on a device architecture of ITO/PEDOT:PSS/$MAPbI_3$/PCBM/Ag (as shown in Figure 8(a))

to evaluate their photovoltaic performance. The comparison of *J-V* curves are shown in Figures 8(b,c). The corresponding photovoltaic data of open-circuit voltage (V_{oc}), short-circuit current density (J_{sc}) and fill factor (FF) was summarized in Table 2. The photovoltaic performance parameters of the best devices based on the conventionally processed perovskite layers are: J_{sc} of 22.19 mA/cm^2, V_{oc} of 1.00 V, FF of 0.672 and the PCE of 14.92%. Figure 8(b) also illustrates that the conventionally processed devices have a relatively large hysteresis, which might originate from the contribution of numerous nanoscale grains in the CB-perovskite layers. Whereas for the simultaneously-formed perovskite solar cells, Figures 8(c,d) show that the devices have a superior photovoltaic performance with forwardly- and reversely-biased PCEs of 16.42% and 16.58%, respectively. The performance of the simultaneously-formed devices is better than that of devices using the conventional method, with higher J_{sc}, V_{oc} and FF. In particular, these devices show a reduced hysteresis while forwardly and reversely scanned. This phenomenon can be explained by two reasons. Firstly, the large grains in PCBM-perovskite films can suppress the internal recombination and leakage current, thereby enhancing the photovoltaic conversion efficiency of the devices. It is reported that most of perovskite solar cells based on large $MAPbI_3$ grains showed higher PCE (from 15%~17%) than that based on small grains, respectively [21,23,29,30]. Secondly, this graded $MAPbI_3$/PCBM heterojunction can favor the charge extraction in inverted structured perovskite solar cells [21]. Consequently, the designed structure and interfaces in the simultaneously-processed perovskite and PCBM layers can achieve an efficient charge extraction from the absorbing to the functional layers [31,32], leading to the comparable photovoltaic performance of devices. It is also noted that in our work this simultaneous formation method significantly reduces the usage of chlorobenze by 80.6%, offering a more facile method on the device fabrication.

Conclusions

In summary, a simple modified antisolvent method was developed to simultaneously process $CH_3NH_3PbI_3$ and PCBM layers for efficient perovskite solar

cells. The introduction of PCBM into the chlorobenzene solution (20 mg/mL) as the antisolvent not only simplified the fabrication process of the inverted-structured devices, but also significantly reduced the usage of the toxic antisolvent chlorobenzene by 80.6%. Meanwhile, the simultaneously-formed $CH_3NH_3PbI_3$ perovskite films achieved a better crystallinity of the structures than that from conventional antisolvent method. Most of the perovskite grain sizes in these film are over 1 μm, with good interfacial structure formed between the absorbing and the electron transport layers. The simultaneously-formed $CH_3NH_3PbI_3$ and PCBM layers showed an excellent optical performance. Perovskite solar cells based on these layers exhibited a higher photovoltaic performance than the conventional method, in which the PCE was up to 16.58% and low hysteresis. Thereby this simultaneous formation method offered a relatively environment-friendly strategy for fabricating efficient halide perovskite solar cells.

Acknowledgement

This work was supported by National Key Research and Development Program of China (Grant No. 2016YFB0402705), PhD Start-up Fund of Natural Science Foundation of Guangdong Province, China (A2017A030310375), National Natural Science Foundation of China (Grant No. 11575118) and Shenzhen Key Lab Fund (ZDSYS20170228105421966), Shenzhen Science & Technology Project (Grant No. JCYJ20170818092745839), Newton Mobility Grant (IE161019) through Royal Society and the National Natural Science Foundation of China, and Royal Academy of Engineering UK-Research Exchange with China and India.

Conflict of Interest

The authors declare no conflict of interest.

Reference

1 P. Gao, M. Grätzel, M. K. Nazeeruddin, Organohalide lead perovskites for photovoltaic applications, *Energy Environ. Sci.* 7(2014) 2448-2463.

2 S. D. Stranks, H. J. Snaith, Metal-halide perovskites for photovoltaic and light-emitting devices, *Nat. Nanotechnol.***2015**, 10(2015) 391-402.

3 Y. Zhao, K. Zhu, Organic–inorganic hybrid lead halide perovskites for optoelectronic and electronic applications, *Chem. Soc. Rev.* **2016**, 45(2016) 655-689.

4 N. Ali, A. Hussain, R. Ahmed, M. K. Wang, C. Zhao, B.Ul Haq; Y.Q.Fu, Advances in nanostructured thin film materials for solar cell applications, *Renewable & Sustainable Energy Reviews* 59(2016) 726-737.

5 W. S. Yang, B.W. Park, E. H. Jung, N. J. Jeon, Y. C. Kim, D. U. Lee, S. S. Shin, J. Seo, E. K. Kim, J. H. Noh, S. I. Seok, Iodide management in formamidinium-lead-halide-based perovskite layers for efficient solar cells, *Science* 356(2017) 1376-1379.

6 F. Huang, A. R. Pascoe, W. Q. Wu, Z. Ku, Y. Peng, J. Zhong, R. A. Caruso, Y. B. Cheng, Effect of the Microstructure of the Functional Layers on the Efficiency of Perovskite Solar Cells, *Adv. Mater.* 29(2017) 1601715.

7 X. Gu, Y. Wang, T. Zhang, D. Liu, R. Zhang, P. Zhang, J. Wu, Z. D. Chen, S. Li, Enhanced electronic transport in Fe^{3+}-doped TiO_2 for high efficiency perovskite solar cells, *J. Mater. Chem. C* 5(2017) 10754-10760.

8 P. Zhang, J. Wu, T. Zhang, Y. Wang, D. Liu, H. Chen, L. Ji, C. Liu, W. Ahmad, Z. D. Chen, S. Li, Perovskite Solar Cells with ZnO Electron‐Transporting Materials. *Adv. Mater.* 30(2018) 1703737.

9 J. H. Im, I. H. Jang, N. Pellet, M. Grätzel, N. G. Park, Growth of $CH_3NH_3PbI_3$ cuboids with controlled size for high-efficiency perovskite solar cells, *Nat. Nanotechnol.* 9(2014) 927-932.

10 M. Xiao, F. Huang, W. Huang, Y. Dkhissi, Y. Zhu, J. Etheridge, A.Gray-Weale, U.Bach, Y. B.Cheng, L. Spiccia, A fast deposition-crystallization procedure for highly efficient lead iodide perovskite thin-film solar cells, *Angew. Chem. Int. Ed.* 53(2014) 9898–9903.

11 M. Liu, M. B. Johnston, H. J. Snaith, Efficient planar heterojunction perovskite solar cells by vapour deposition *Nature* 501(2013), 395-398.

12 S. Paek, P. Schouwink, E. N. Athanasopoulou, K. T. Cho, G. Grancini, Y. Lee, Y. Zhang, F. Stellacci, M. K. Nazeeruddin, P. Gao, From Nano- to Micrometer Scale: The Role of Antisolvent Treatment on High Performance Perovskite Solar Cells, *Chem. Mater.* 29(2017) 3490-3498.

13 T. Bu, L.Wu, X. Liu, X. Yang, P. Zhou, X. Yu, T. Qin, J. Shi, S. Wang, S. Li, Z. Ku, Y. Peng, F. Huang, Q. Meng, Y. B. Cheng, J. Zhong, Synergic Interface Optimization with Green Solvent Engineering in Mixed Perovskite Solar Cells, *Adv. Energy Mater.* 20(2017) 1700576.

14 M. Habibi, F. Zabihi, M. R. Ahmadian-Yazdi, M. Eslamian, Progress in emerging solution-processed thin film solar cells – Part II: Perovskite solar cells, *Renewable and Sustainable Energy Reviews* 62(2016) 1012-1031.

15 T. Baikie, Y. Fang, J. M. Kadro, M. Schreyer, F. Wei, S. G. Mhaisalkar, M. Graetzel, T. J. White, Synthesis and crystal chemistry of the hybrid perovskite $(CH_3NH_3)PbI_3$ for solid-state sensitised solar cell applications, *J. Mater. Chem. A* 1(2013) 5628-5641.

16 M.-R. Ahmadian-Yazdi, M. Habibi, M. Eslamian, Excitation of Wet Perovskite Films by Ultrasonic Vibration Improves the Device Performance, *Appl. Sci.*, 8(2018) 308.

17 Y. Wang, J. Wu, P. Zhang, D. Liu, T. Zhang, L. Ji, X. Gu, Z. D. Chen, S. Li, Stitching triple cation perovskite by a mixed anti-solvent process for high performance perovskite solar cells, *Nano Energy* 39 (2017) 616–625.

18 Y. Wang, T. Zhang, P. Zhang, D. Liu, L. Ji, H. Chen, Z. D. Chen, J. Wu, S. Li, Solution processed PCBM-$CH_3NH_3PbI_3$ heterojunction photodetectors with enhanced performance and stability, *Org. Electron.* 57(2018) 263-268.

19 C. Lan, S. Zhao, C.Zhang, W.Liu, S.Hayase, T. Ma, Concentration gradient-controlled growth of large-grain CH3NH3PbI3 films and enhanced photovoltaic performance of solar cells under ambient conditions, *CrystEngComm* 18(2016) 9243.

20 D. Bi, C. Yi, J. Luo,J. D. Décoppet, F. Zhang,S.M. Zakeeruddin,X. Li,A. Hagfeldt, M. Grätzel, Polymer-templated nucleation and crystal growth of perovskite films

for solar cells with efficiency greater than 21%, *Nature Energy* 1(2017) 16142.

21 Y. Wu, X. Yang, W. Chen, Y. Yue, M. Cai, F. Xie, E. Bi, A. Islam, L. Han, Perovskite solar cells with 18.21% efficiency and area over 1 cm2 fabricated by heterojunction engineering, *Nat. Energy* 1(2016) 16184.

22 F. Zhang, W. Shi, J. Luo, N. Pellet, C. Yi, X. Li, X. Zhao, T. John S. Dennis, X. Li, S. Wang, Y. Xiao, S. M. Zakeeruddin, D. Bi, M. Grätzel, Isomer-Pure Bis-PCBM-Assisted Crystal Engineering of Perovskite Solar Cells Showing Excellent Effciency and Stability, *Adv. Mater.* 29(2017) 1606806.

23 S. Yoon, M.-W. Ha, D.-W. Kang, PCBM-blended chlorobenzene hybrid anti-solvent engineering for efficient planar perovskite solar cells, *J. Mater. Chem. C* 5(2017) 10143-10151.

24 Y. X. Zhao, K. Zhu, Three-step sequential solution deposition of PbI2-free $CH_3NH_3PbI_3$ perovskite, *J. Mater. Chem. A* 3 (2015) 9086-9091.

25 D.-Y. Son, J.-W. Lee, Y. J. Choi, I.-H. Jang, S. Lee, P. J. Yoo, H. Shin, N. Ahn, M. Choi, D. Kim, N.-G. Park, Self-formed grain boundary healing layer for highly efficient $CH_3NH_3PbI_3$ perovskite solar cells, *Nat. Energy* 1(2016) 16081.

26 Q. Dong, Y. Fang, Y. Shao, P. Mulligan, J. Qiu, L. Cao, J. Huang, Electron-hole diffusion lengths > 175 μm in solution-grown $CH_3NH_3PbI_3$ single crystals, *Science* 347(20155), 967-970.

27 D. W. Quilettes, S. M. Vorpahl, S. D. Stranks, H. Nagaoka, G. E. Eperon, M. E. Ziffer, H. J. Snaith, D. S. Ginger, Impact of microstructure on local carrier lifetime in perovskite solar cells, *Science* 348(2015) 683-686.

28 S. Li, P. Zhang, H. Chen, Y. Wang, D. Liu, J. Wu, H. Sarvari, Z. D. Chen,Mesoporous PbI2 assisted growth of large perovskite grains for efficient perovskite solar cells based on ZnO nanorods,J. Power Sources 342(2017) 990-997.

29 Q. Wang, C.-C. Chueh, T. Zhao, J. Q. Cheng, M. Eslamian, W. C. H. Choy, A. K.-Y. Jen, Effects of Self-Assembled Monolayer Modification of Nickel Oxide Nanoparticles Layer on the Performance and Application of Inverted Perovskite Solar Cells, *ChemSusChem* 10(2017) 3794-3803.

30 Q. Wang, F. Lin, C.-C. Chueh, T. Zhao, M. Eslamian, A. K.-Y. Jen, Enhancing

efficiency of perovskite solar cells by reducing defects through imidazolium cation incorporation, *Materials Today Energy* 7(2018) 161-168.

31 Y. Rong, Y. Hu, S. Ravishankar, H. Liu, X. Hou, Y. Sheng, A. Mei, Q. Wang, D. Li, M. Xu, J. Bisquert, H. Han, Tunable hysteresis effect for perovskite solar cells *Energy Environ. Sci.* 10(2017) 2383-2391.

32 G. Yang, H. Tao, P. Qin, W. Ke, G. Fang, Recent progress in electron transport layers for efficient perovskite solar cells *J. Mater. Chem. A* 4(2016) 3970-3990.

Figures Captions

Figure 1. Schematic of simultaneous formation of perovskite and PCBM layers: (a) Simultaneous formation method; (b) Conventional antisolvent method.

Figure 2.XRD patterns of films that were prepared through simultaneous formation and conventional antisolvent methods.

Figure 3. Top-view SEM images of films: (a) CB-perovskite film prepared from 200 ul of CB; (b) CB-perovskite film prepared from 60 ul of CB; (c) perovskite+PCBM films prepared from 250 ul of CB antisolvent; (d) grain size statistics extracted from Figure 3(a). (scale bar 200 nm)

Figure 4. Top-view SEM images of films: (a) PCBM-Perovskite films; (b) CB-rinsed PCBM-perovskite films; (c) CB-rinsed perovskite+PCBM films; (d) grain size statistics extracted from Figure 4(b). (scale bar 200 nm)

Figure 5. Cross-sectional SEM image of PCBM-Perovskite films prepared from 60 ul of PCBM-CB antisolvent.(The thickness of PCBM layer is appr. 60 nm, and the thickness of perovksite layer is appr. 300 nm).

Figure 6. UV-vis spectra of PCBM-perovskite, CB-perovskite and Perovskite+PCBM films: (a) Reflectance; (b) Transmittance; (c) Absorptions.

Figure 7. TRPL lifetime of perovskite/PCBM films prepared through different

methods.

Figure 8. (a) Architecture of the devices; (b) reverse scan J-V characteristics of perovskite solar cells fabricated through simultaneous formation and conventional antisolvent methods; (c) forward- and reverse-scanned J-V curves of simultaneously-formed perovskite solar cells; (d) histogram of forward scan PCE values for 20 simultaneously-formed perovskite solar cells.

Table 1.XRD parameters extracted from Figure 2 based on PCBM-perovskite, CB-perovksite films and perovskite+PCBM, repectively.

	2 theta	FWHM (deg.)	Intensity (a.u.)	Crystalline size (nm)
PCBM-perovskite	14.10	0.346	7279	22.75
CB-perovskite	14.09	0.371	3566	21.21
perovskite+PCBM	14.09	0.381	3427	20.66

Table 2. Photovoltaic data of perovskite solar cells extracted from Figures 6b and 6c based on PCBM-perovskite and perovskite+PCBM films, respectively.

Films	scan direction	J_{sc}(mA/cm^2)	V_{oc}(V)	FF	*PCE*(%)
PCBM-perovskite	forward	23.39	1.01	0.695	16.42
	reverse	23.12	1.00	0.717	16.58
perovskite+PCBM	forward	23.21	0.97	0.604	13.61
	reverse	22.19	1.00	0.672	14.92

Highlights

1. High-quality perovskite and PCBM layers are simultaneously formed for efficient solar cells.
2. Device fabrication was simplified in simultaneous formation method.
3. Compared to conventional antisolvent method, the use of toxic solvent was reduced.

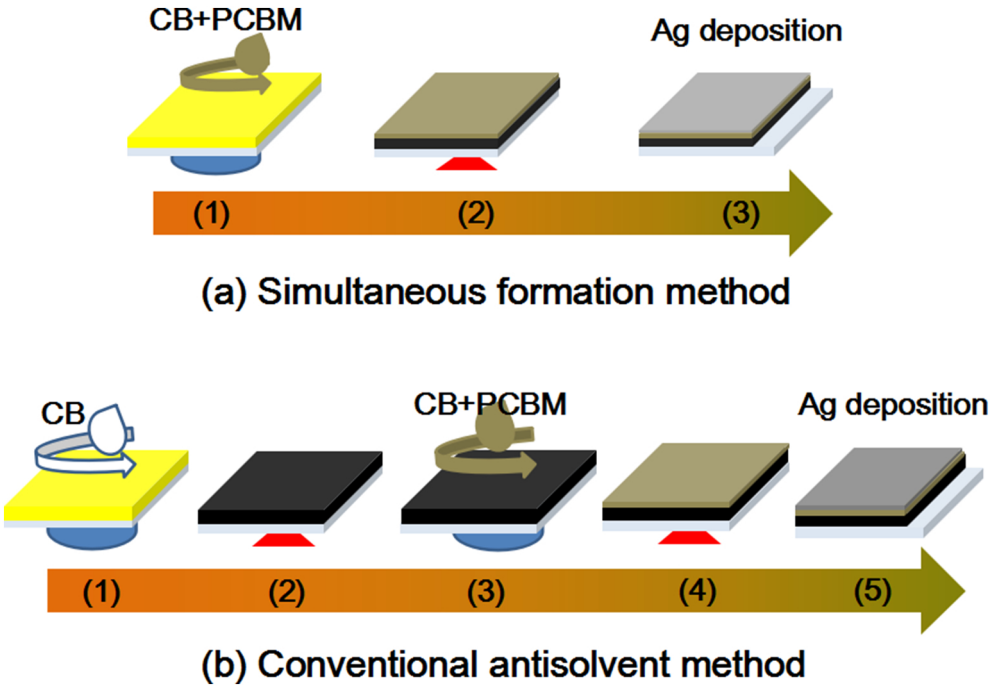
CB+PCBM
Ag deposition
(1)
(2)
(3)
(a) Simultaneous formation method
CB
CB+PCBM
Ag deposition
(1)
(2)
(3)
(4)
(5)
(b) Conventional antisolvent method

Figure 1

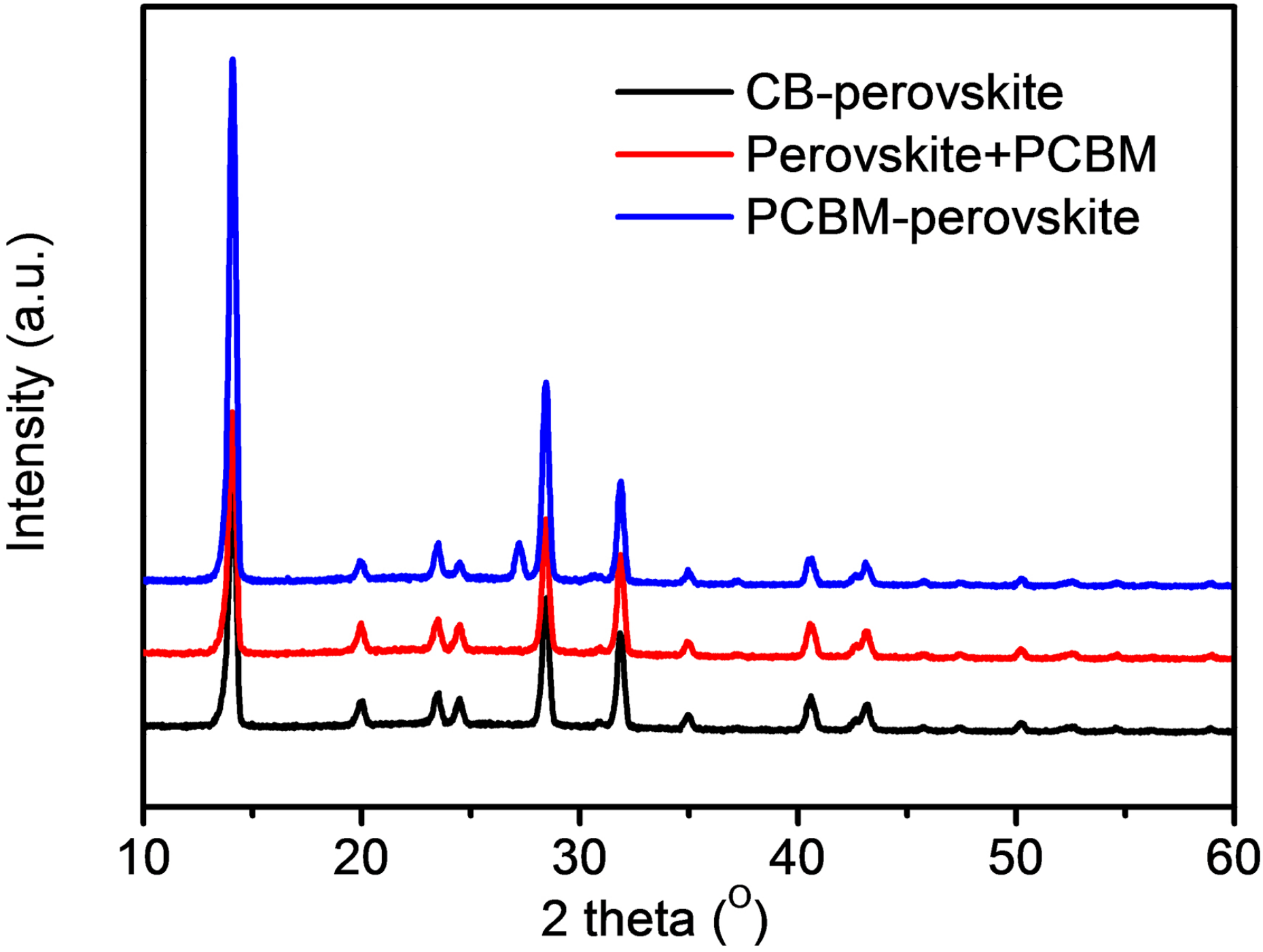
CB-perovskite
Perovskite+PCBM
PCBM-perovskite
Intensity (a.u.)
10
20
30
40
50
60
2 theta (O)

Figure 2

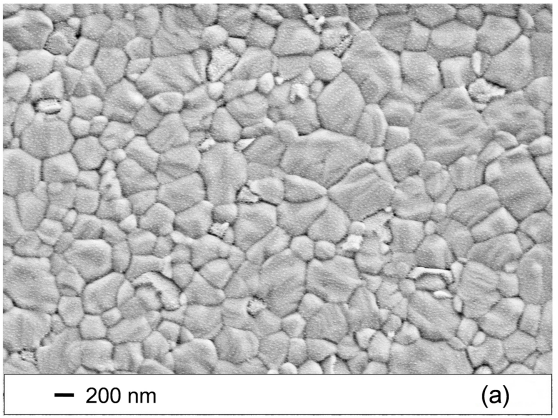
200 nm
(a)

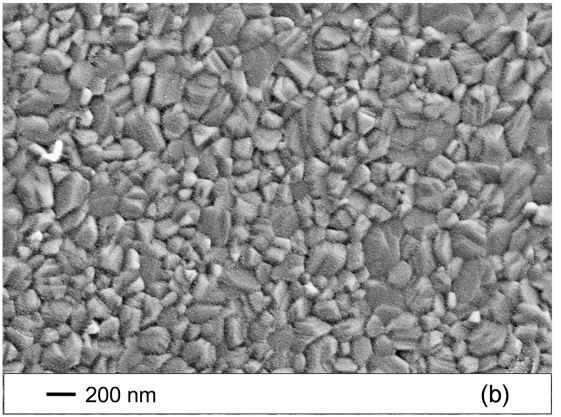
200 nm
(b)

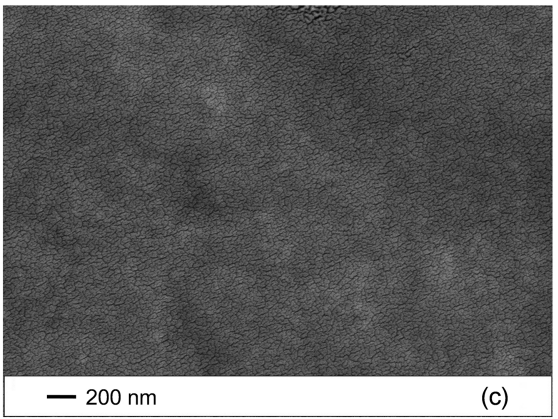
200 nm
(c)

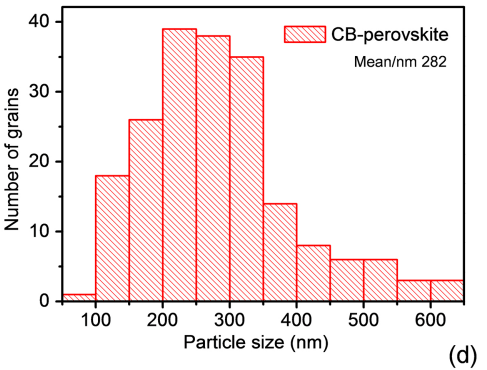
CB-perovskite
Mean/nm 282
Number of grains
Particle size (nm)
0
10
20
30
40
100
200
300
400
500
600
(d)

Figure 3

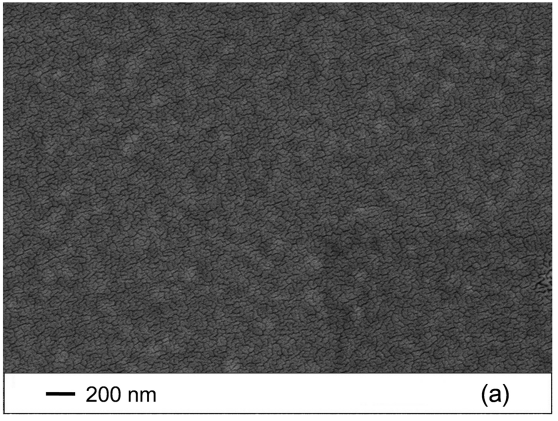
200 nm
(a)

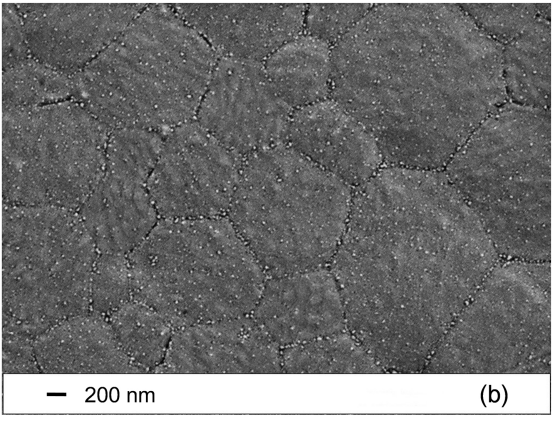
200 nm
(b)

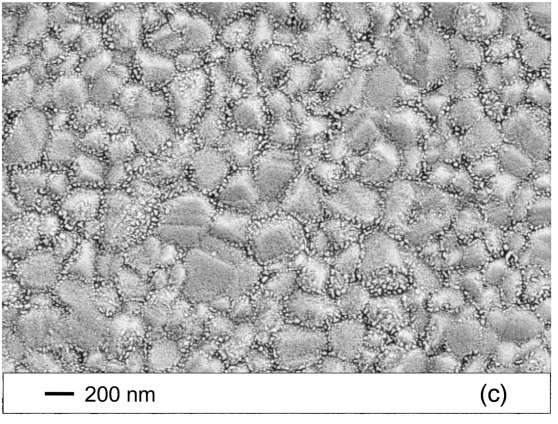
200 nm
(c)

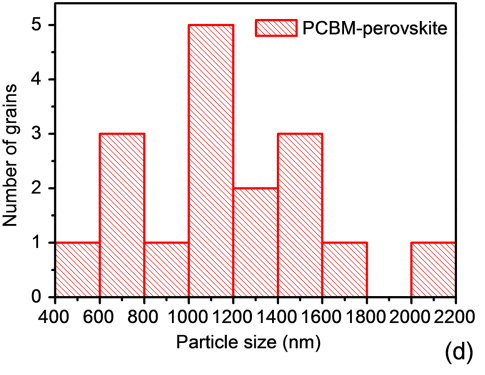
PCBM-perovskite
Number of grains
0
1
2
3
4
5
400
600
800
1000
1200
1400
1600
1800
2000
2200
Particle size (nm)
(d)

Figure 4

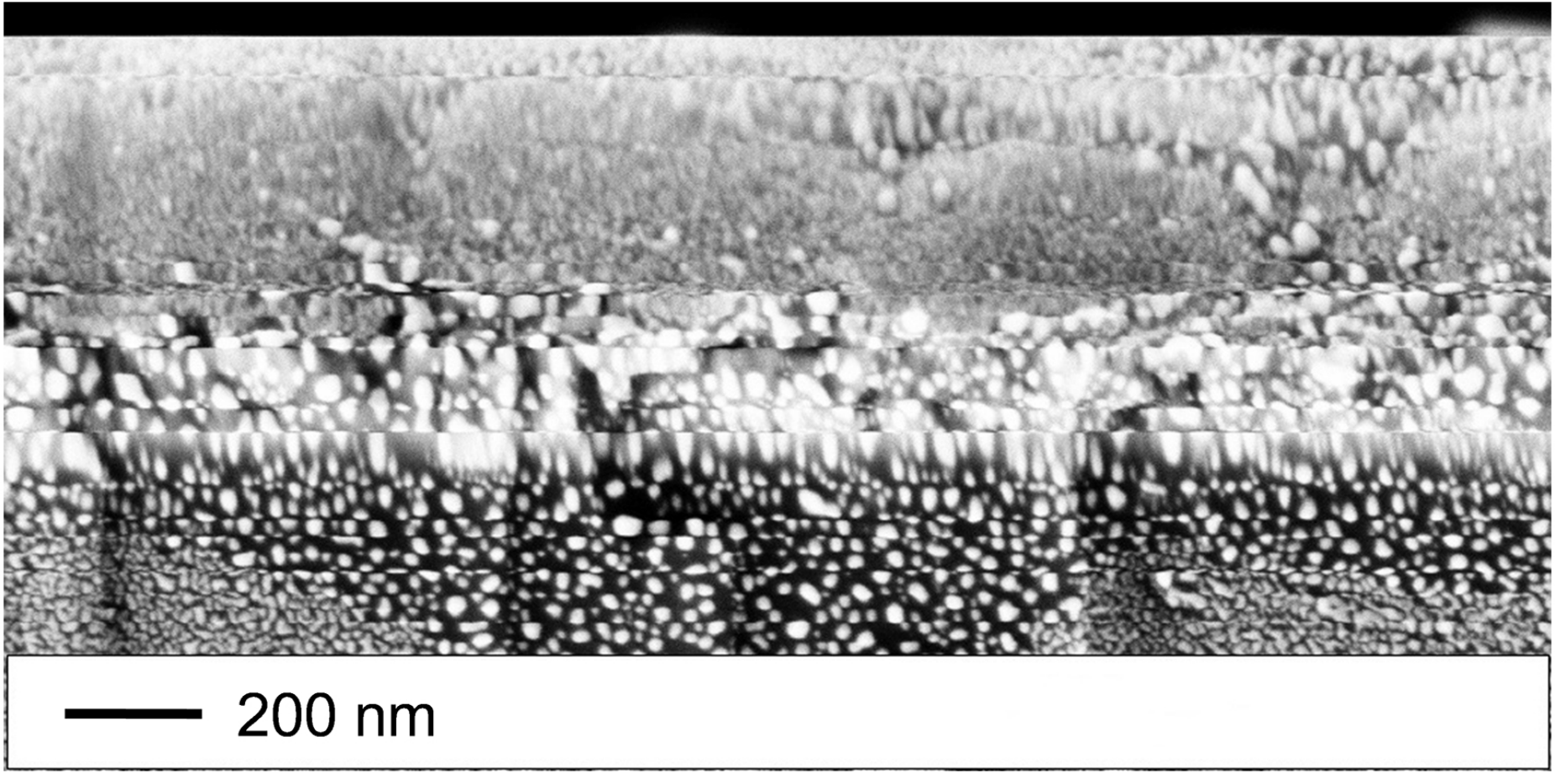

Figure 5

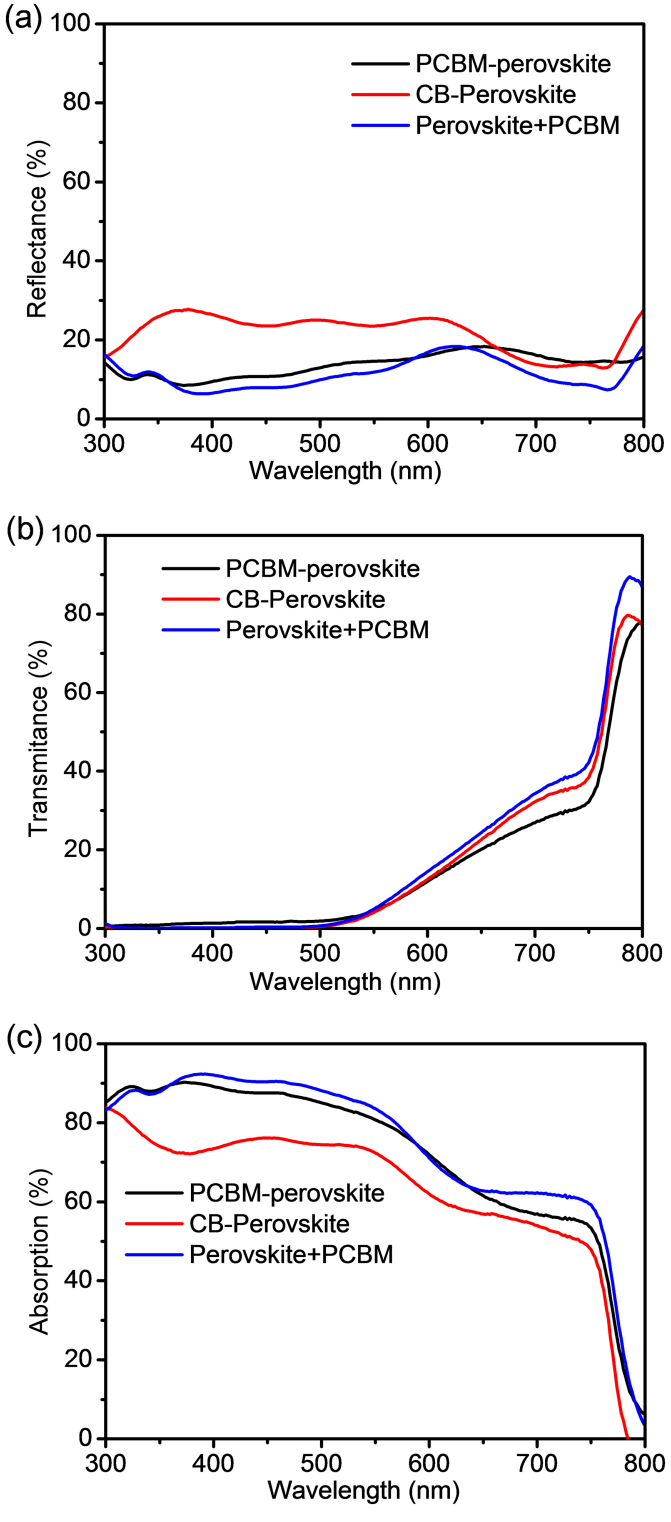
(a)
Reflectance (%)
Wavelength (nm)
PCBM-perovskite
CB-Perovskite
Perovskite+PCBM
(b)
Transmitance (%)
Wavelength (nm)
PCBM-perovskite
CB-Perovskite
Perovskite+PCBM
(c)
Absorption (%)
Wavelength (nm)
PCBM-perovskite
CB-Perovskite
Perovskite+PCBM

Figure 6

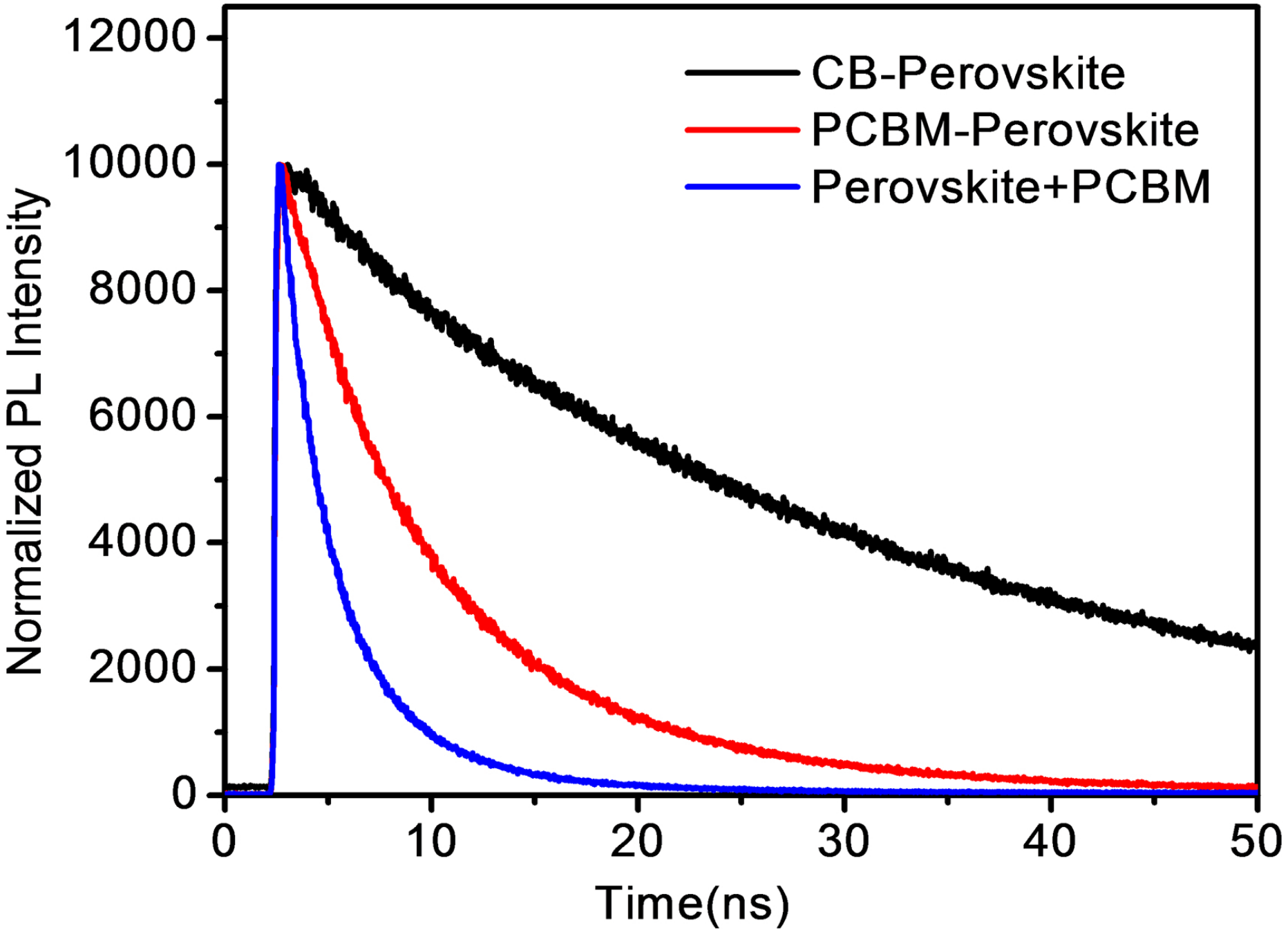
12000
10000
8000
6000
4000
2000
0
Normalized PL Intensity
0
10
20
30
40
50
Time(ns)
CB-Perovskite
PCBM-Perovskite
Perovskite+PCBM

Figure 7

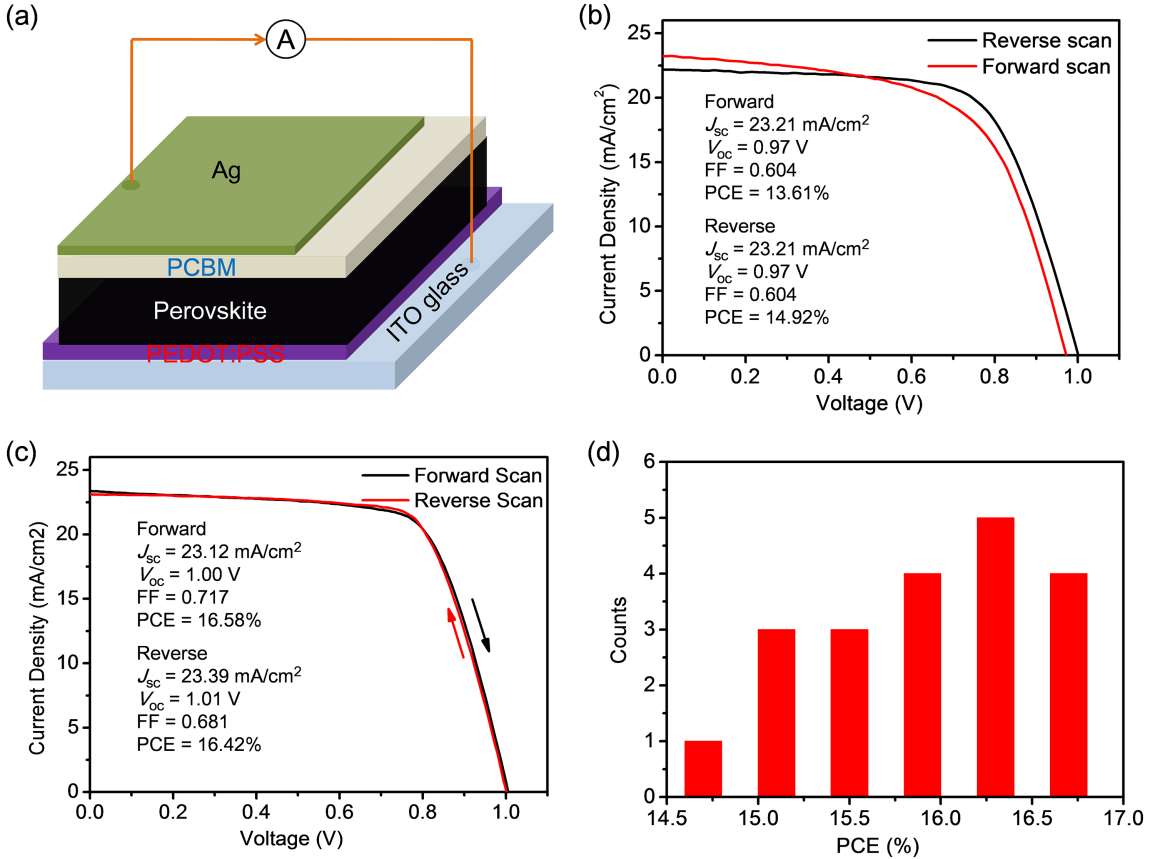
(a)
A
Ag
PCBM
Perovskite
PEDOT:PSS
ITO glass
(b)
Reverse scan
Forward scan
Forward
J_{sc} = 23.21 mA/cm^2
V_{oc} = 0.97 V
FF = 0.604
PCE = 13.61%
Reverse
J_{sc} = 23.21 mA/cm^2
V_{oc} = 0.97 V
FF = 0.604
PCE = 14.92%
Current Density (mA/cm^2)
Voltage (V)
(c)
Forward Scan
Reverse Scan
Forward
J_{sc} = 23.12 mA/cm^2
V_{oc} = 1.00 V
FF = 0.717
PCE = 16.58%
Reverse
J_{sc} = 23.39 mA/cm^2
V_{oc} = 1.01 V
FF = 0.681
PCE = 16.42%
Current Density (mA/cm2)
Voltage (V)
(d)
Counts
PCE (%)

Figure 8